Am J Cancer Res 2024;14(3):1101-1120
www.ajcr.us /ISSN:2156-6976/ajcr0150675

Original Article

Nanostructured lipid carriers loaded with morellic acid for enhanced anticancer efficacy: preparation, characterization, pharmacokinetics and anticancer evaluation

Buyun Jia[1,4*], Shanshan Li[2,4*], Lu Li[1], Tongsheng Wang[1,4], Weidong Chen[3,4], Guangliang Chen[1,4]

[1]College of Integrative Medicine, Anhui University of Chinese Medicine, Hefei, Anhui, China; [2]School of Traditional Chinese Medicine, Anhui University of Chinese Medicine, Hefei, Anhui, China; [3]College of Pharmacy, Anhui University of Chinese Medicine, Hefei, Anhui, China; [4]Anhui Province Key Laboratory of Chinese Medicinal Formula, Hefei, Anhui, China. [*]Equal contributors and co-first authors.

Received April 12, 2023; Accepted February 26, 2024; Epub March 15, 2024; Published March 30, 2024

Abstract: Morellic acid (MA), a typical compound found in Garcinia plants, is known for its anticancer properties. In present study, we isolated MA from resin of *Garcinia hanburyi Hook. f.* using preparative chromatography. We have successfully prepared MA-loaded nanostructured lipid carriers (MA-NLCs) and refined the production process via orthogonal testing. Optimization of the preparation process resulted in an average particle size of 165.50±1.70 nm with a PDI of 0.19±0.01. The EE% and DL% of MA-NLCs were 78.17±0.34% and 7.25±0.38%, respectively. The zeta potential of MA-NLCs was -21.85±0.67 mV. Comparatively, MA-NLCs showed a greater area under the curve (AUC) and an extended half-life (t1/2) than free MA. Pharmacokinetics analysis revealed that the AUC_{0-t} increased from 4.91±0.65 μg/mL·min (free MA) to 18.91±3.40 μg/mL·min (MA-NLCs) and the $t_{1/2}$ value for MA-NLCs was 7.93-fold longer than that of free MA. *In vitro* cytotoxic assessments indicated that MA formulations curtailed the proliferation of cancer cells. *In vivo*, MA-NLCs significantly inhibited the tumor growth in tumor-bearing mouse model. Molecular mechanism studies revealed that up-regulation of apaf-1 and activation of caspase-3, caspase-9 and GSDME by MA-NLCs may trigger to apoptosis and pyroptosis in cancer cells. Consequently, our findings support the potential of NLCs as an effective MA delivery system for the clinical management of cancer.

Keywords: Morellic acid, extraction and isolation, nanostructured lipid carriers, pharmacokinetics, anticancer activity

Introduction

Garcinia xanthones, a special class of compounds with notable anticancer properties, have attracted increased attention worldwide [1]. Morellic acid (MA) a typical garcinia plant derivative, shares a similar chemical structure and biological activities with gambogic acid (GA), as illustrated in **Figure 1A** and **1B** [2]. Previous studies showed that MA inhibited proliferation of various tumor cell lines, including HT-29, COL-2, BCA-1, LU-1, HeLa, and HCT-116 [3]. The anti-tumor activity of MA may result from its anti-angiogenesis activity [4]. However, use of MA has been limited by its pharmacokinetic characteristics, such as short elimination half-life and poor water solubility [5]. Lipid nanoparticulate systems (LNS) such as solid lipid nanoparticles (SLNs) and nanostructured lipid carriers (NLCs) have been developed as innovative drug delivery systems (DDS) in recent decades [6]. SLNs are composed of solid lipids, whereas NLCs integrate both solid and liquid lipids, offering a disordered internal structure that mitigates the risk of drug leakage and gelation associated with the ordered structure of SLNs [7]. LNS can improve the bioavailability of drugs and control release, particularly for drugs that are poorly permeable and hydrophobic [8]. For anticancer therapy, LNS allowed for targeting of anticancer agents, potentially increasing permeability and retention (EPR) at tumor tissues and improving tumor cellular uptake [9]. Therefore, the combination of LNS and natural

https://doi.org/10.62347/VBOX7111

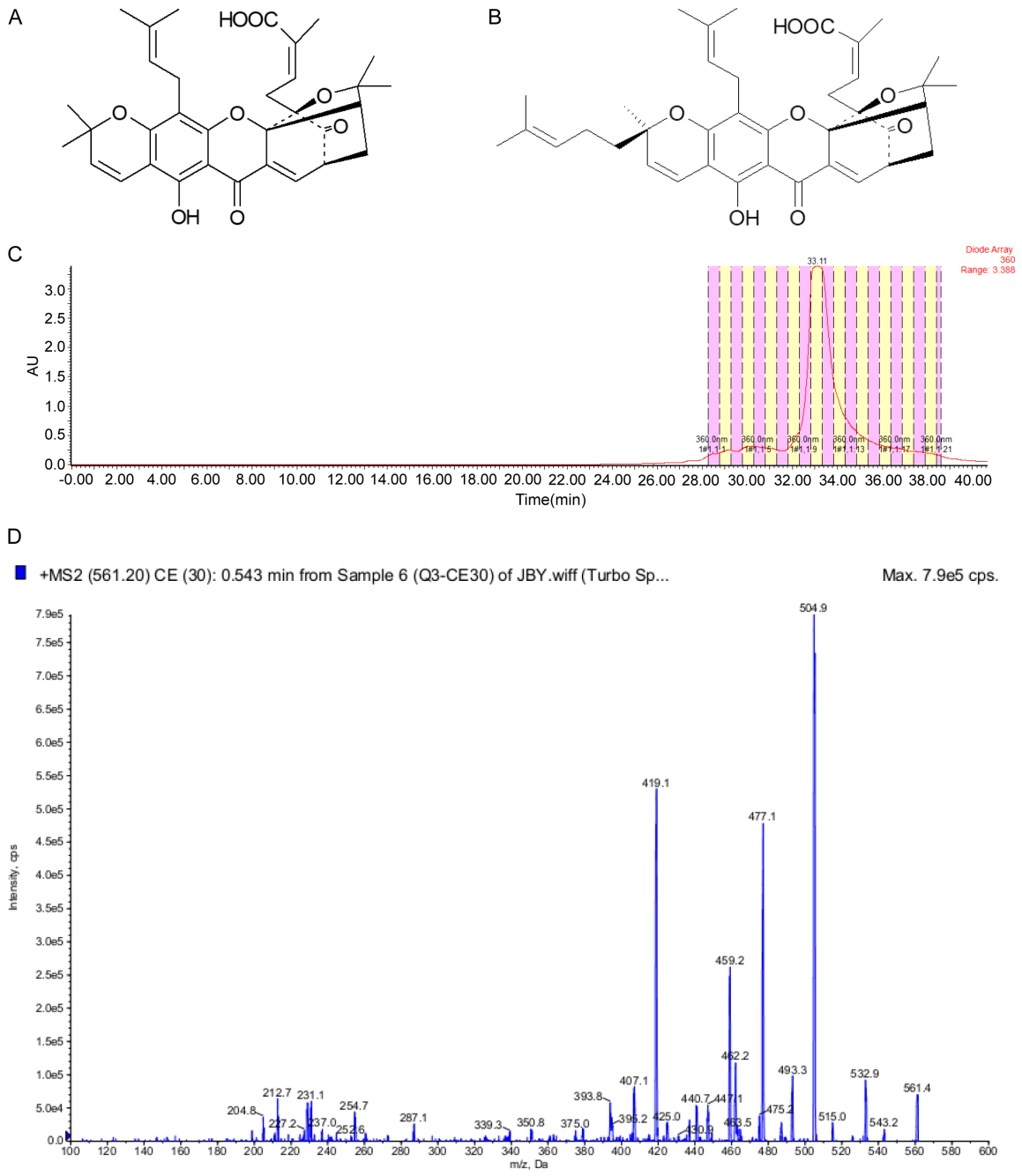

Figure 1. Chemical structure and isolation of MA. A. Chemical structure of MA; B. Chemical structure of GA; C. Chromatogram of preparative HPLC; D. Chromatogram of HPLC-MS/MS of MA at positive ion model.

anti-cancer agents will represent an optimal system for cancer treatment.

In this study, we isolated MA from resin of Garcinia hanburyi Hook. f. via ultrasonic extraction and preparative chromatography. The preparation process for MA-loaded nanostructured lipid carriers (MA-NLCs) was optimized, and the resulting product was characterized using scanning electron microscopy (SEM). We evaluated particle size, zeta potential, Encapsulation efficiency (EE%), drug loading (DL%), and performed differential scanning calorimetry (DSC). Furthermore, we investigated the pharmacokinetics of MA-NLCs in Sprague Dawley (SD) rats, and evaluated toxicity of this formulation against several cancer cell lines *in vitro*. *In vivo* antitumor efficacy was investigat-

ed in tumor-bearing BALB/c mouse model. Additionally, we investigated the apoptotic and pyroptotic pathways induced by MA-NLCs, examining the potential involvement of proteins such as apaf-1, caspase-9, caspase-3, and GSDME.

Materials and methods

Materials

MA (≥98.0%) was isolated from dry resin of *Garcinia hanburyi Hook. f.* Gambogic acid was provided by the National Institutes for Food and Drug Control (Beijing, China). Lecithin was a gift from Jiangsu Kangyuan Pharmaceutical Co., Ltd. (Lianyungang, China). Pluronic F68 (F68) was purchased from BASF SE (Germany). Tween 80 was purchased from Sinopharm Chemical Reagent Co., Ltd. (Shanghai, China). Glyceryl monostearate (GMS) was obtained from Anhui Shenying Pharmaceutical Co., Ltd. (Hefei, China). Medium chain triglyceride (MCT) was obtained from Croda (United Kingdom). Annexin V/PI was obtained from Bestbio Biotechnology (Shanghai, China). Apaf-1, caspase-9, caspase-3 and GSDME antibody were obtained from Zen-Bioscience (Chengdu, China). All other reagents used in this study were analytical grade and deionized distilled water (ddH_2O) was employed as well. Sprague Dawley rats (180-200 g, 8 weeks) were used for evaluation of pharmacokinetics and BALB/c mouse (18-20 g, 8 weeks) were used for *in vivo* antitumor study. All tumor cell lines were purchased from Shanghai Institute of Biochemistry and Cell Biology, Chinese Academy of Sciences (Shanghai, China).

Extraction and isolation of MA

Dry resin of Garcinia hanburyi were extracted in ethanol (3 × 0.4 L) with ultrasonication at 40°C. The ethanol extract was fractionated using medium pressure semi-preparative chromatography with MeOH:water (80:20) as the mobile phase to yield four fractions. The first fraction was further separated into several compounds by preparative HPLC using MeOH:water (90:10) as the mobile phase. Eluted MA was concentrated under reduced pressure, which resulted in orange powder. The structure of MA was determined using mass spectrometry, IR, ^{1}H-NMR, and ^{13}C-NMR [3].

Preparation of MA and GA solutions

MA solution was dissolved in a mixture of ethanol:PEG200:0.9% NaCl solution (5:25:70, v/v/v). This solution was used as a reference formulation for MA-NLCs in *in vitro* release study, pharmacokinetics study, cytotoxicity study and *in vivo* antitumor study. GA solution was prepared in the same liquid system that used to prepare the MA solution, and was used as a positive control in the cytotoxicity study.

Preparation of MA-NLCs

In this study, we prepared MA-NLCs using an emulsion-evaporation and low temperature solidification method [10]. A mixture of MA, GMS, MCT, and lecithin was dissolved in organic solvent and incubated in water bath at 68±2°C (organic phase). In addition, F68 and Tween 80 were dissolved in water and incubated in a water bath at 68±2°C (aqueous phase). Following thermal equilibration of the organic and aqueous phases, the organic phase was rapidly added to the aqueous phase with stirring at 900 rpm. After continuous stirring for three hours, the pre-emulsion was introduced into chilled water (0-2°C), followed by an additional hour of stirring to yield the colloidal MA-NLCs. We optimized preparation conditions and prescription proportions including emulsification time (h), solidification time (h), stirring speed (rpm), ratio of organic solvent (ethanol:acetone, v/v), proportion of F68 and Tween-80 (w/w), amount of surfactant (w%), proportion of organic and aqueous phases (v/v), amount of MCT in total lipid (w%), proportion of drug and lipid (w/w), proportion of emulsion and ice-water for solidification (v/v), and amount of lecithin (w%) with EE% of MA in MA-NLCs as the primary output. The preparation process was further optimized using an orthogonal test with a weighted score of EE% and DL% as outputs (weighted score = EE% × 0.8 + DL% × 0.2) and factors of orthogonal test were selected according to the result of the above formulation preparation optimization. Furthermore, a verification test was introduced to test the reproducibility of the optimized preparation process.

Preparation of MA loaded solid lipid nanoparticles (MA-SLNs)

In this study, MA-SLNs was used as a reference formulation and prepared by a method which was established in our previous study [8]. Specifically, a mixture of MA (10 mg), GMS (200 mg) and lecithin (100 mg) were dissolved in a mix solution of acetone (4 mL) and alcohol (1

mL), and incubated in water bath at 70±2°C (organic phase). In addition, F68 (2.4 w/v%) and Tween 80 (1.2 w/v%) were dissolved in water and incubated in a water bath at 70±2°C (aqueous phase). Following thermal equilibration of the organic and aqueous phases, the organic phase was rapidly added to the aqueous phase with stirring at 1000 rpm. After stirring at 70±2°C for 3 h, the pre-emulsion was poured into cold water (0-2°C), then stirred at 1000 rpm for 1 h to obtain colloidal MA-SLNs.

Preparation of MA-NLCs lyophilized powder and MA-SLNs lyophilized powder

We used a lyophilizer to prepare the MA-NLCs lyophilized powder and MA-SLNs lyophilized powder. Five percent mannitol was added to colloidal MA-NLCs or MA-SLNs. Colloidal MA-NLCs or MA-SLNs were separated into multiple glass bottles and pre-frozen at -20°C for 12 h. Then, the samples were placed in a lyophilizer and freeze-dried at -70°C for 24 h to obtain a lyophilized powder.

Scanning electron microscopy

The morphology of MA-NLCs was evaluated using SEM. Colloidal MA-NLCs was placed on copper grids and dried at room temperature prior to visualization [11].

Evaluation of particle size and zeta potential

The average particle size and zeta potential of MA-NLCs were measured using a Zeta-sizer NanoZs (3000HS, Malvern Instruments Ltd., UK) at room temperature. All samples were diluted with ddH_2O and subsequently analyzed in triplicate [6].

Encapsulation efficiency and drug loading

The EE% and DL% were determined using a mini sephadax G-50 column (1.0 cm × 15.0 cm) with centrifugation [12]. 100 mL of colloidal MA-NLCs was added to the top of a mini sephadax G-50 column, and 1 mL of ddH_2O was used as eluent. The column was then centrifuged at 1,000 rpm for 3 mins, and unencapsulated MA molecules were retained on the column. The eluate was diluted with ethanol to a final volume of 10 mL. The amount of encapsulated MA was determined by HPLC.

The EE% and DL% of MA-NLCs were determined using the following equations:

$$EE\% = \frac{W_E}{W_A} \times 100\%$$

$$DL\% = \frac{W_E}{W_E + W_L} \times 100\%$$

Where W_E represents the amount of MA encapsulated in the NLCs, W_A represents the initial amount of MA, and W_L represents the amount of lipid added to the system.

Differential scanning calorimetry analysis

In this study, DSC analysis was performed using a Q2000 DSC detector (American TA Instrument Co., Ltd., New Castle, DE) to obtain thermograms of MA-NLCs. Samples were placed in aluminum pans, which were heated from 20°C to 250°C at a rate of 10°C /min [13]. Thermograms were recorded for (a) MA, (b) GMS, (c) F68, (d) Lecithin, (e) a physical mixture of GMS, F68, lecithin, and MA, and (f) MA-NLCs (lyophilized powder).

Stability of MA-NLCs

Stability of MA-NLCs was evaluated at 4°C and 25°C. At each time point, EE% and particle size were evaluated at 0, 10, 15, 20, 25, 30, 35, 40, 45 and 60 d [14].

In vitro release of MA-NLCs

In vitro release was evaluated using a dialysis bag with phosphate buffered saline (PBS, pH=7.4) containing 0.5% sodium dodecyl sulfate (SDS). 5 mL of the MA-NLC suspension and an equivalent volume of the MA solution were each transferred into individual dialysis bags. The dialysis bags were placed in 100 mL of release medium and stirred at 100 rpm at 37±0.5°C. 1 mL of release medium was sampled, with replacement, at 5, 10, 15, 30, 45, 60, 90, 150, 180, 240, 300, 540, 720, 1,440, and 2,880 mins. The samples were analyzed using HPLC [15].

In vivo pharmacokinetics

12 SD rats were randomly divided into two groups that received either intravenous MA solution or intravenous MA-NLCs. Both groups received a MA dose of 3 mg/kg (The concentra-

tion of MA Solution or MA-NLCs were 3 mg/mL, therefore the injection volume was 1 mL/kg). Following administration, 0.1 mL of blood was collected from the retro-orbital plexus at 5, 10, 20, 30, 60, 90, 120, 180, 240, 360, 480, 600, and 720 mins. Blood samples were centrifuged at 3,000 rpm for 10 mins to obtain plasma, which was frozen at -20°C until HPLC analysis [16]. The experimental protocol was approved by the Institutional Ethical Committee of Anhui University of Chinese Medicine, Hefei, China.

In vitro cytotoxicity

Cytotoxicity was evaluated against cells including BEL-7402, BEL-7402/ADR, HepG2, A549, B16, AGS, HGC-27, MKN-45, MFC and 4T1 using the 3-(4, 5-dimethlthizo(-2-yl)-2, 5-diphenyltrazolium bromide assay (MTT assay)) [17]. MA and GA were dissolved in DMSO. MA-SLNs and MA-NLCs were dissolved in PBS solution. All cells were cultured in DMEM at 37°C in a 5% CO_2 atmosphere. All experiments were performed on cells during the logarithmic growth phase. Cells were seeded in 96-well plates at a concentration of 5.0×10^5 cells/mL. MA formulations and GA were added at 0.1, 0.25, 0.5, 1, 2, 4, 8, 10, and 20 μM. After 24 h, the cells were incubated with MTT (5 mg/mL) in DMEM at 37°C for 4 h. The medium was then removed and 200 μL of DMSO was added to each well. The absorbance in each well was determined using a microplate reader at 570 nm. The inhibition rates (IR%) of the MA formulations were determined using the following equation:

$$IR\% = \frac{OD_C - OD_S}{OD_C} \times 100\%$$

Where OD_c represents the absorbance of the negative control group and ODs represents the absorbance of MA formulations.

In vivo antitumor study

The MFC tumor-bearing BALB/c mouse model was created following prior protocols. Briefly, male BALB/c mice were subcutaneously injected with 1×10^5 MFC cells in the right axilla. When tumors grew to approximately 50 mm^3, mice were randomly sorted into 5 groups (n= 10 each): a control group receiving normal saline, a positive control group receiving 5-Fu (100 mg/kg; The concentration of 5-Fu was 40 mg/mL, therefore the injection volume was 2.5 mL/kg), and three drug groups treated with either MA Solution, MA-SLNs or MA-NLCs at 2 mg/kg MA equivalent (The concentration of MA Solution, MA-SLNs or MA-NLCs were 0.8 mg/mL, therefore the injection volume was 2.5 mL/kg). Tail vein injections were administered every other day for 15 d. Body weights and tumor volumes (calculated using the formula $V = ab^2/2$, where 'a' is the major axis and 'b' is the minor axis measured by calipers) were recorded every 5 d post-administration. At the final day of the experiment, mice were sacrificed, and the tumors were excised, weighed, and photographed. Inhibition ratio (IR) was computed using the formula: IR (%) = [(x - y)/x] × 100%, with 'x' and 'y' denoting the average tumor weight for the control and treatment groups, respectively. The tumor tissue samples were collected for further staining and assay. The experimental protocol was approved by the Institutional Ethical Committee of Anhui University of Chinese Medicine, Hefei, China.

Hematoxylin and eosin (H&E) staining of tumor tissue

The tumor tissue samples were fixed in 4% paraformaldehyde, embedded in paraffin, and sectioned into 5 μm thick slices. The prepared sections were subsequently mounted on glass slides, stained with hematoxylin and eosin, and examined microscopically to assess histopathological alterations within the tumor tissue samples.

Immunohistochemistry (IHC) of tumor tissue

The tumor tissue samples were fixed in 4% paraformaldehyde and processed into paraffin sections. These sections were then dewaxed using dimethyl benzene and gradient ethanol, followed by a PBS wash (10 mM, pH 7.2). Subsequently, the samples underwent a 15-min incubation in 3% H_2O_2 (v/v) at 25°C, followed by two 4-min boiling steps in citric acid buffer. After blocking with 5% bovine serum albumin for 20 mins, the samples were incubated overnight at 4°C with primary antibodies. The sections were then washed four times with PBS and incubated with goat anti-rabbit IgG (1:100) at 37°C for 30 mins. Finally, the slides were counterstained with DAB and examined using a light microscope.

Cell apoptosis assay

Cancer cells were seeded in 6-well plates at a concentration of 1.0×10^6 cells/mL and incu-

bated at 37°C in a 5% CO_2 atmosphere for 24 h. Then cancer cells were treated with free MA solution and MA-NLCs at MA concentrations of 1 μM and 2 μM, and the untreated cells were used as a control. After MA formulations treatment for 24 h, cancer cells were digested with EDTA-free trypsin and washed with chilled PBS. Then 400 μL of binding buffer was added to each well and then the cells were stained with 5 μL of Annexin V-FITC for 15 mins and 10 μL of propidium iodide for 5 mins at 4°C in the dark. The flow cytometry analysis was performed and data was analyzed using Flowjo software.

Lactate dehydrogenase (LDH) release

In this study, we used LDH assay kit to evaluate the impact of MA-NLCs treatment on LDH release in cancer cells. Cells were seeded in 96-well plate at a density of 5×10^4 cells/well and incubated for 24 h. MA solution, MA-SLNs and MA-NLCs at 2 μM MA equivalent were introduced to the cells for 24 h, while untreated cells served as the control. Cellular LDH release levels were measured following the instructions of the LDH assay kit at 0 h, 12 h, 24 h, and 48 h post-treatment.

Western blot assay

Cells were seeded in 10 cm dishes at a density of 1×10^7 and incubated for 24 h. MA solution, MA-SLNs and MA-NLCs at 2 μM MA equivalent were introduced to the cells for 24 h, while untreated cells served as the control. The cells were rinsed with PBS three times and then lysed in RIPA buffer with 1% proteinase inhibitor. The protein concentration was determined using the BCA Protein Assay kit. After mixing with protein loading buffer, the samples were heated in 100°C for 8 mins. Tumor tissue samples were homogenized and processed in a manner akin to the aforementioned method to extract total protein. The protein (15 μg) was separated through 10% SDS-PAGE and transferred onto nitrocellulose membranes. The membranes were obstructed with a 5% milk solution in TBST, followed by an overnight incubation with primary antibodies at 4°C. Subsequently, the membranes were washed 3 times with TBST and incubated with secondary antibodies for 1 h. Finally, the bands were visualized using an enhanced chemiluminescence (ECL) kit. The levels of the target proteins were standardized based on the reference bands of β-actin.

Analysis of MA using HPLC

Determination of MA concentration was performed using a Shimadzu LC-20C HPLC system (Shimadzu, Japan) equipped with UV-Vis detector operated at 360 nm. Samples were separated on a Shimadzu stainless steel C18 reversed phase column (250 × 4.60 mm) packed with 5-μm particles. The mobile phase was methanol:water (90:10, v/v) at a flow rate of 1.000 mL/min.

Statistical analysis

Data in this study were calculated using GraphPad Prism 6.0. All results were presented as the mean ± SD. Groups were compared using t-tests or one-way ANOVA. $P<0.05$ or $P<0.01$ was considered statistically significant.

Results

Extraction and isolation of MA

We have isolated MA from resin of Garcinia hanburyi successfully. Purified MA was obtained from the eluent corresponding to the peak of retention time 32.30 to 34.30 min (**Figure 1C**). The sample was analyzed using HPLC-MS in positive ion mode, which resulted in a peak for MA at m/z 561.4 (Calcd for $C_{33}H_{36}O_8$: 561.4) (**Figure 1D**).

Evaluation using IR resulted in identification of the following peaks and functional groups: IR (KBr): 3080 cm^{-1} (-OH), 2976 cm^{-1} (-CH3), 2928 cm^{-1} (-CH2-), 1435 cm^{-1} (-CH3, -CH2-), 1364 cm^{-1} (-CH3), 3360 cm^{-1} (-COOH), 1690 cm^{-1} (C=O), 1651, 1593, and 1435 cm^{-1} (-Ar).

The ^{1}H-NMR and ^{13}C-NMR data were as follows: ^{1}H-NMR: (MeOD, 400 MHz) δ7.56 (1H, d, J=6.8 Hz), 6.57 (1H, d, J=10.0 Hz), 5.96 (1H, t, J=7.0 Hz), 5.44 (1H, d, J=10.0 Hz), 5.08 (1H, s), 3.45 (1H, dd, J=6.4, 4.8 Hz), 3.29 (2H, m), 2.91 (2H, m), 2.59 (2H, m), 2.36 (1H, s), 1.79 (1H, dd, J=13.6, 4.5 Hz), 1.76 (3H, s), 1.68 (3H, s), 1.64 (3H, s), 1.61 (3H, s), 1.43 (3H, s), 1.39 (3H, s), 1.26 (3H, s), 1.03 (1H, s). ^{13}C-NMR: (MeOD, 100 MHz) δ205.49, 181.22, 170.66, 162.64, 159.41, 159.01, 137.74, 137.54, 135.14, 132.66, 129.86, 127.73, 124.23, 116.87, 109.75, 104.57, 101.28, 92.92, 85.56, 85.42, 80.20, 50.74, 30.99, 30.91, 29.56, 29.36, 29.20, 26.48, 23.26, 21.87, 19.04, 18.91, 13.40.

Selection of preparation conditions and prescription proportions

We optimized formulation preparation according to our pre-study and previous studies. A mixture of MA (5.0 mg), GMS (80.0 mg), MCT (20.0 mg), and lecithin (100 mg) was dissolved in organic solvent (2.5 mL) and incubated in a water bath at 68±2°C to obtain the organic phase. Concurrently, F68 (100 mg) and Tween-80 (100 mg) were dissolved in pure water (10 mL) and incubated in a water bath at 68±2°C to obtain the aqueous phase. Upon reaching equilibrium, the organic phase was rapidly added to the aqueous phase with continuous stirring at 900 rpm. After stirring for 3 h, the pre-emulsion was introduced into cold water (30 mL, 0-2°C), followed by stirring in an ice bath at 900 rpm for one hour to produce the colloidal MA-NLCs.

The EE% of MA-NLCs increased with increased emulsification time (**Figure 2A**), solidification time (**Figure 2B**), and stirring speed (**Figure 2C**), then reached a plateau when these values reached 3 h, 1 h and 1,000 rpm, respectively. The emulsification time was set at 3 h, the solidification time was set at 1 h, and the stirring speed was set at 1,000 rpm. Further experiments indicated that while increased acetone volume expedited the drying of organic solvents, it did not enhance the formation of MA-NLCs (**Figure 2D**). Leading to the selection of ethanol as the preferred organic solvent. In addition, the EE% was maximal when F68 and Tween-80 were included at a 1:1 ratio (**Figure 2E**). Ratios of organic to aqueous phase at 1:4 and 1:10 (**Figure 2G**) resulted in the highest EE%. However, the 1:10 proportion resulted in a large volume when the volume of organic phase was fixed, which presented a barrier to freeze-drying. Consequently, a 1:4 ratio was standardized. We also found that a 1:3 proportion of emulsion to ice water resulted in maximal EE% (**Figure 2J**). Additionally, MCT in total lipid (**Figure 2H**), proportion of drug and lipid (**Figure 2I**), amount of surfactant (**Figure 2F**), and amount of lecithin (**Figure 2K**), each increased the EE% up to a point before decreasing. Therefore, an orthogonal test was performed to further optimize the preparation of MA-NLCs.

Orthogonal test

We conducted optimization of the MCT content in total lipid (A), ratio of drug to lipid (B), amount of lecithin (C), and amount of surfactant (D) using an orthogonal procedure with a weighted score of EE% and DL% as outputs (weighted score = EE% × 0.8 + DL% × 0.2). The levels of each factor were determined from prior formulation optimization. The findings, arranged by the impact on the preparation of MA-NLCs, are detailed in **Table 1**, with the rank order being A>B>D>C. Analysis of variance indicated that the levels of A and B were significantly different. The results indicated that the optimal formulation conditions for MA-NLCs preparation were $A_2B_2C_2D_1$, which comprises 20% MCT in total lipid, a 1:20 drug:lipid ratio, 1.5% lecithin, and 2.5% surfactant. Therefore, the optimized formulation was prepared as following: MA (5.0 mg), GMS (80.0 mg), MCT (20.0 mg), and lecithin (150 mg) were dissolved in alcohol (2.5 mL) and incubated in a water bath at 68±2°C to produce organic phase. Concurrently, F68 (125 mg) and Tween-80 (125 mg) were dissolved in of pure water (10 mL) and incubated in a water bath at 68±2°C to obtain the aqueous phase. Following equilibration, the organic phase was rapidly mixed with the aqueous phase under stirring at 900 rpm. Following 3 hours of stirring, the pre-emulsion was poured into cold water (30 mL, 0-2°C) and incubated in an ice bath with stirring at 1,000 rpm for 1 h to acquire colloidal MA-NLCs.

Verification test

Using the optimized process and formulation, we prepared three batches of MA-NLCs in parallel and measured the EE% and DL%. The EE% and DL% of the prepared MA-NLCs were 78.26±0.95% and 3.63±0.04% with relative standard deviations of 1.22% and 1.13%, respectively (**Table 2**). These results indicated that preparation of MA-NLCs was reproducible.

Characterization of MA-NLCs

SEM analysis revealed that the MA-NLCs were spherical with particle sizes below 200 nm (**Figure 3A1**, **3A2**). The particle size and zeta potential of the MA-NLCs were immediately assessed post-preparation using a Zetasizer. As shown in **Figure 3B** and **Table 3**, MA-NLCs had an average particle size of 165.50±1.70 nm and an average PDI of 0.19±0.01. Zeta potential is indicative of colloidal solution stability to a certain extent. The preferred ranges of zeta potential values for nanoparticle stability merely by electrostatic repulsion are >20 mV

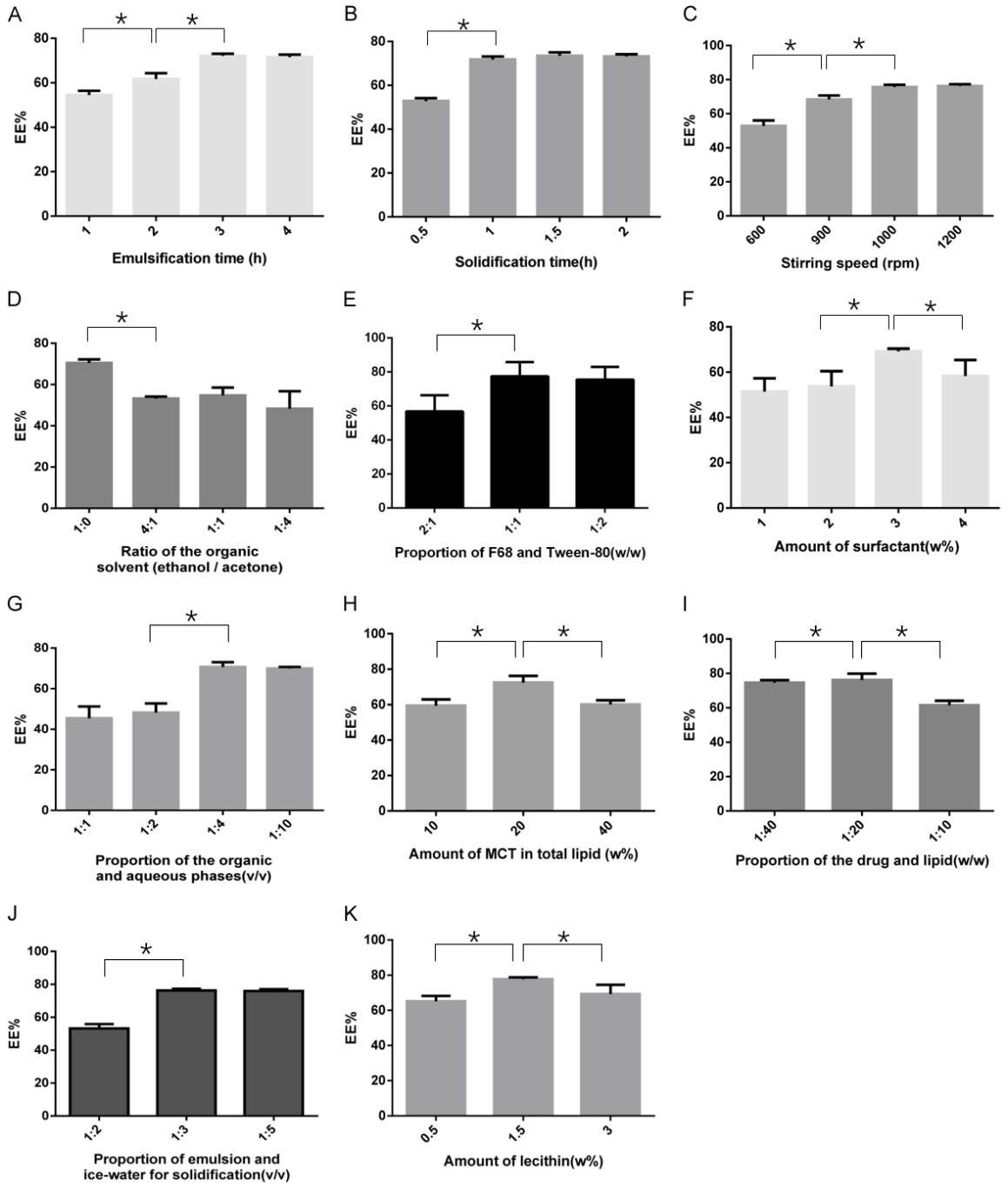

Figure 2. Selection of preparation condition and prescription proportion (n=3). A. Selection of emulsification time (h); B. Selection of solidification time (h); C. Selection of stirring speed (rpm); D. Selection of stirring ratio of the organic solvent (ethanol/acetone) (v/v); E. Selection of proportion of F68 and Tween-80 (w/w); F. Selection of amount of surfactant (w%); G. Selection of proportion of the organic and aqueous phases (v/v); H. Selection of amount of MCT in total lipid (w%); I. Selection of proportion of the drug and lipid (w/w); J. Selection of proportion of emulsion and ice-water for solidification (v/v); K. Selection of amount of lecithin (w%). *P<0.05.

and <-20 mV. The zeta potential of MA-NLCs was -21.85±0.67 mV. The EE% and DL% of prepared MA-NLCs were 78.17±0.34% and 7.25±0.38%, respectively. DSC analysis was performed to evaluate thermal characteristics of MA-NLCs. As shown in **Figure 3C**, MA exhib-

Table 1. Arrangement and results of orthogonal test

Test No.	Factors				DL%	EE%	Weighted Score
	(A) Amount of MCT in total lipid (%)	(B) Proportion of the drug and lipid (w/w)	(C) Amount of lecithin (%)	(D) Amount of surfactant (%)			
1	15	1:25	1	2.5	1.50	61.08	49.17
2	15	1:20	1.5	3	3.17	65.47	53.01
3	15	1:15	2.5	3.5	5.85	62.13	50.87
4	20	1:25	1.5	3.5	1.81	73.56	59.21
5	20	1:20	2.5	2.5	3.82	79.36	64.25
6	20	1:15	1	3	6.93	74.48	60.97
7	25	1:25	2.5	3	1.76	71.54	57.58
8	25	1:20	1	3.5	3.75	77.91	63.07
9	25	1:15	1.5	2.5	6.97	74.97	61.37
K1	51.017	55.320	57.737	58.263			
K2	61.477	60.110	57.863	57.187			
K3	60.673	57.737	57.567	57.717			
R	10.460	4.790	0.296	1.076			
SSE	203.308	34.417	1.739	0.130			
Variance	2.000	2.000	2.000	2.000			
F ratio	1528.632	258.774	1.000	13.075			
P	<0.05	<0.05	>0.05	>0.05			

Abbreviations: DL%: drug loading (%); EE%: encapsulation efficiency (%); K1: average score of level 1 of corresponding factors; K2: average score of level 2 of corresponding factors; K3: average score of level 3 of corresponding factors; R: range of the average score of each factor; SSE: Sum of Squares due to Error.

Table 2. Results of verification test

Batches	EE%	DL%
1	79.18	3.67
2	78.34	3.63
3	77.27	3.63
Mean ± SD	78.26±0.95	3.63±0.04
RSD%	1.22	1.13

Abbreviations: DL%, drug loading (%); EE%, encapsulation efficiency (%); RSD%, relative standard deviation (%).

ited a sharp melting peak at 108.75°C. The melting peaks of GMS and F68 were at 62.36°C and 55.45°C, respectively. The physical mixture of the individual components of MA-NLCs displayed two additional melting peaks, whereas the MA-NLCs themselves had a distinct peak at 49.71°C.

Stability of MA-NLCs

A short-term stability study was performed by storing MA-NLCs colloidal solution at 4°C and 25°C for 45 d. As shown in **Figure 4A** and **4B**, an upward trend of average particle size and a downward trend of EE% were observed at 25°C, but these trends were not observed at 4°C.

In vitro release study

In vitro release of MA and MA-NLCs was determined by using dialysis. As shown in **Figure 4C**, the cumulative release rate of free MA was 97.52% at 7 h. In contrast, MA-NLCs continuously released MA for 48 h. These results indicated that free MA reached 80% release within 2 h and was nearly completely released at 7 h. The MA-NLCs formulation demonstrated more sustained release *in vitro*, with 55.15% drug release within the initial 7 h, followed by slow and sustained release over the next 40 h.

In vivo pharmacokinetics

The concentration-time curves of MA and MA-NLCs are presented in **Figure 4D**, and the pharmacokinetic parameters are listed in **Table 4**. The mean residence time (MRT) in the MA-NLCs group was higher than that observed for the free MA group (191.31±27.58 mins vs 23.94±2.24 mins, $P<0.05$). Clearance (CL) of the MA-NLCs formulation was significantly slower than that of free MA ($P<0.05$). Encapsulation of MA in NLCs significantly increased systemic drug exposure, as evidenced by an

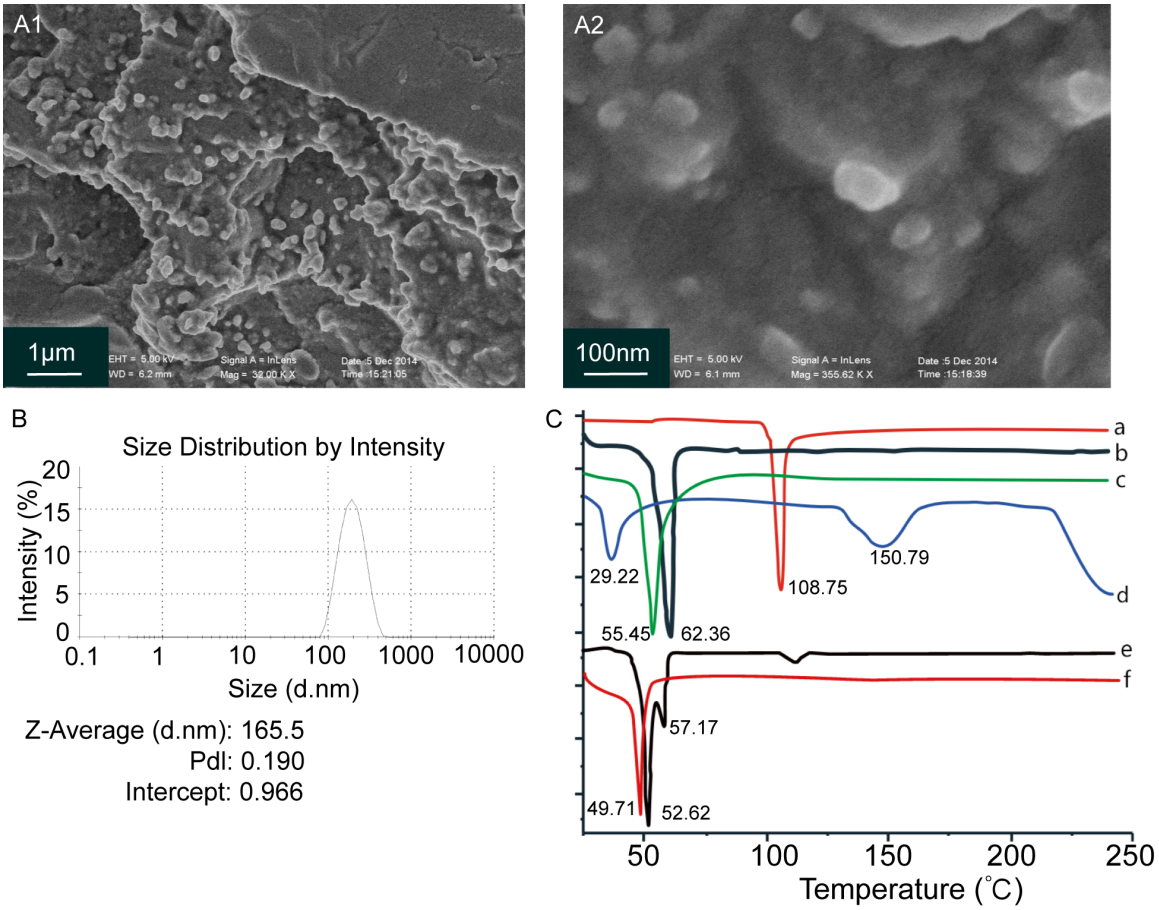

Figure 3. Characterization of MA-NLCs. A1. SEM of MA-NLC; A2. Detail of SEM of MA-NLC; B. Particle size and PDI of MA-NLCs; C. DSC analysis. (a) MA, (b) GMS, (c) F68, (d) Lecithin, (e) Physical mixture of GMS, F68, lecithin and MA, (f) MA-NLCs.

Table 3. Characterization of MA-NLCs (Mean ± SD, n=3)

Sample	Particle size (nm)	PDI	Zeta potential (mV)	EE%	DL%
MA-NLCs	165.50±1.70	0.19±0.01	-21.85±0.67	78.17±0.34	7.25±0.38

Abbreviations: PDI, polydispersity index; EE%, encapsulation efficiency (%); DL%, drug loading (%).

increase in AUC from 4.91±0.65 μg/mL·min to 18.91±3.40 μg/mL·min. In addition, the $t_{1/2}$ value of MA-NLCs was 7.93-fold longer than that of free MA. An increased MRT indicated that MA, when encapsulated in NLCs, circulates in the bloodstream for an extended period. Furthermore, increased AUC indicated that MA-NLCs had higher relative bioavailability than free MA, which indicated that MA-NLCs promoted sustained release of MA.

In vitro cytotoxicity

The MTT assay results revealed that free MA curbed the growth of cancer cells, with half-maximal inhibitory concentration (IC_{50}) values of 7.96±0.23 μM for BEL-7402 cells, 14.14±1.17 μM for BEL-7402/ADR cells, 10.39±1.02 μM for HepG2 cells, 5.19±0.34 μM for A549 cells, 4.24±0.11 μM for B16 cells, 2.93±0.51 μM for AGS cells, 6.11±0.19 μM for HGC-27 cells, 2.13±0.05 μM for MKN-45 cells, 4.91±0.07 μM for MFC cells, and 9.84±0.37 μM for 4T1 cells, respectively. Antiproliferative efficacy was augmented by encapsulation of MA in NLCs, as demonstrated by decreased IC_{50} values in all cell lines. In comparison with gambogic acid (GA) solution, the positive control, MA exhibited a better *in vitro* anticancer activity against MKN-45 and B16 cells (**Table 5**).

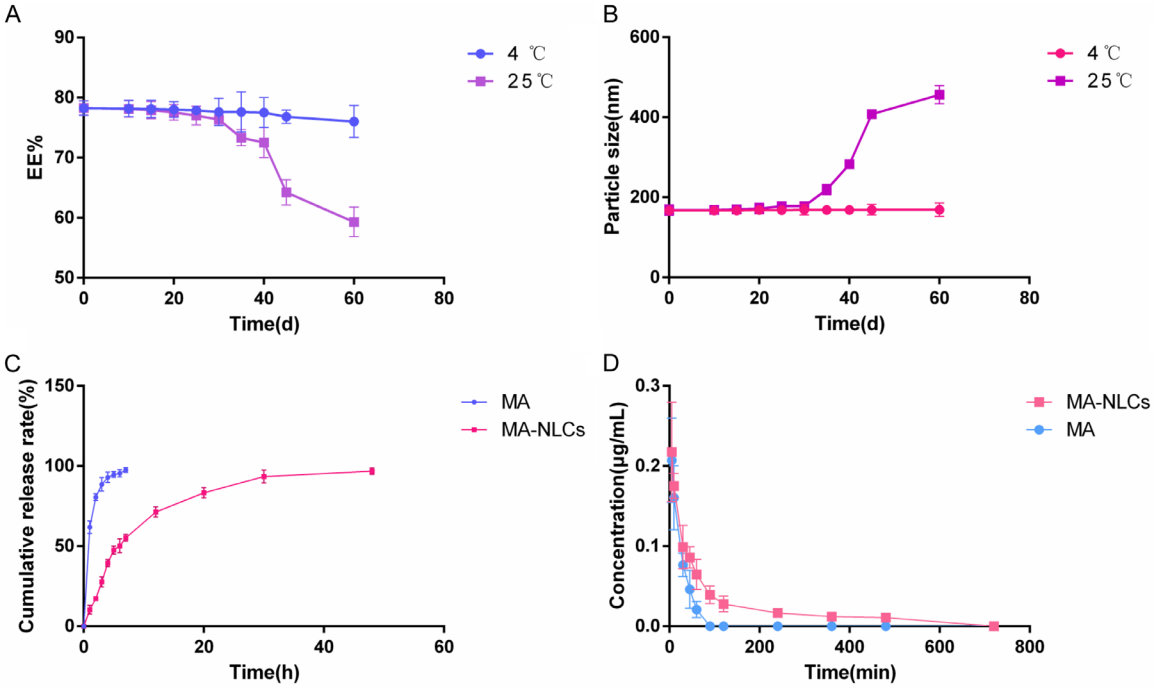

Figure 4. Stability and release kinetics of MA-NLCs (A-C: n=3, D: n=6). (A) Changes of EE% of MA-NLCs at 4 °C and 25 °C; (B) Changes of MS of MA-NLCs at 4 °C and 25 °C; (C) The profiles of *in vitro* release of MA and MA-NLCs; (D) Concentration-time curve of single i.v. administration of MA and MA-NLCs.

Table 4. Pharmacokinetics parameters of single i.v. administration of MA solution and MA-NLCs (Mean ± SD, n=6)

Parameters	Unit	Formulations	
		MA	MA-NLCs
$t_{1/2\alpha}$	min	2.97±0.63	17.18±1.61*
$t_{1/2\beta}$	min	21.06±3.25	167.05±12.07*
Vd	(mg/kg)/(μg/mL)	6.24±0.81	14.69±0.99*
CL	(mg/kg)/(μg/mL)/min	0.69±0.07	0.14±0.05*
C_{max}	μg/mL	0.35±0.10	0.29±0.13
AUC_{0-t}	μg/mL·min	4.91±0.65	18.90±3.40*
AUC_{0-inf}	μg/mL·min	5.05±0.87	20.11±1.89*
MRT	min	23.93±2.24	191.31±27.58*

Abbreviations: MA, morellic acid; MA-NLCs, MA-loaded nanostructured lipid carriers; $t_{1/2\alpha}$, distribution half-life; $t_{1/2\beta}$, elimination half-life; Vd, apparent volume of distribution; CL, clearance; AUC, area under curve; MRT, mean residence time. *P<0.05 compared to the MA group.

Furthermore, MA-NLCs exhibited greater cytotoxicity than free MA and MA-SLNs against each of the 10 cancer cell lines at equivalent MA concentrations (**Figure 5**).

In vivo antitumor efficacy

In vivo antitumor efficacy of MA-NLCs was investigated in MFC tumor-bearing BALB/c mouse model. Compared with model group, the growth of the tumors was significantly inhibited in MA group, MA-SLNs group and 5-Fu group. The tumor volumes in the MA-NLCs group were much smaller than those of MA group and MA-SLNs group ($P<0.05$ or $P<0.01$), indicating an improved antitumor effect of MA-NLCs compared to the MA and MA-SLNs (**Figure 6A-C**). The tumor weight in model group, MA group, MA-SLNs group, MA-NLCs group and 5-Fu group were 2.24±0.57 g, 1.21±0.45 g, 1.02±

Table 5. IC_{50} of MA formulations and GA against different cancer cell lines (Mean ± SD, n=3)

Cell lines	IC_{50} values (μM)			
	MA	MA-SLNs	MA-NLCs	GA
BEL-7402	7.96±0.23	5.08±0.21	3.40±0.13	0.98±0.05
BEL-7402/ADR	14.14±1.17	10.48±0.98	9.29±0.45	9.52±0.77
HepG2	10.39±1.02	8.26±0.54	6.07±0.11	6.68±0.21
A549	5.19±0.34	2.65±0.77	1.75±0.17	1.47±0.04
B16	4.24±0.11	3.57±0.24	2.89±0.39	4.99±0.38
AGS	2.93±0.51	1.95±0.16	1.02±0.02	1.47±0.06
HGC-27	6.11±0.19	4.49±0.13	3.31±0.14	3.67±0.11
MKN-45	2.13±0.05	1.71±0.04	0.94±0.06	4.04±0.08
MFC	4.91±0.07	2.44±0.09	2.05±0.33	3.59±0.12
4T1	9.84±0.37	7.34±0.73	6.38±0.19	3.83±0.30

Abbreviations: MA, morellic acid; MA-SLNs, MA-loaded solid lipid nanoparticles; MA-NLCs, MA-loaded nanostructured lipid carriers; GA, gambogic acid.

0.40 g, 0.61±0.37 g and 0.35±0.18 g, respectively (**Figure 6D**). The inhibition ratio (IR) calculated from tumor weight in these groups were 45.97±5.34%, 54.33±7.94%, 72.95±9.20%, and 84.42±17.65%, respectively (**Figure 6E**). Compared with the normal group, the mice in free MA group, MA-SLNs or MA-NLCs group did not show a significant decrease in body weight while 5-Fu caused apparent weight loss (**Figure 6F**).

H&E staining

After H&E staining of the tumor tissue sections, the cell nuclei appeared blue, whereas the cytoplasm was stained light purple. In the tumor tissues of model group, the nuclei of tumor cells were densely packed with intact nuclei, while the tumor tissues of MA group displayed scattered apoptotic and necrotic cells, intercellular clefts, and nuclear characteristics indicative of condensation and fragmentation. These phenomena were more evident in the MA-NLCs group (**Figure 6G**).

IHC analysis

To further estimate the antitumor efficacy of MA-NLCs, immunohistochemistry analysis was performed to determine the apoptosis-related proteins Ki67 in tumors. As depicted in **Figure 6H**, MA significantly reduced the expression of the proliferation marker Ki67, an effect that was amplified when MA was delivered using MA-NLCs. These results further corroborate the enhanced antitumor efficacy of MA-NLCs (**Figure 6H**).

Assessment of apoptosis by Annexin-V/PI staining

In order to further estimate the anticancer efficacy of MA and MA-NLCs, the cancer cells apoptosis was measured by Annexin-V/PI staining. When treated with different concentration of MA and MA-NLCs for 24 h, the apoptotic rate of MKN-45 cells was increased in a dose dependent manner: The apoptotic rate increased from 3.17±0.06% (Con.) to 36.2±0.32% (MA, 2 μM) and 3.03±0.06% (Con.) to 77.4±0.44% (MA-NLCs, 2 μM). Notably, the apoptotic rate of MA-NLCs group was much higher than that of MA group at the same concentration of MA (**Figure 7A**).

LDH release study

The results of the LDH release assay indicated that MA formulations significantly enhanced LDH release in MKN-45 and MFC cells (**Figure 7B**). When compared to the MA group and MA-SLNs group, MA-NLCs displayed a stronger effect in increasing cellular LDH release levels (**Figure 7B**). These results suggested that MA-NLCs has a stronger impact on inducing cell death in gastric cancer cells compared to MA and MA-SLNs, potentially through the induction of pyroptosis.

MA-NLCs induces changes in the levels of apoptosis and pyroptosis related proteins

We evaluated the effects of MA-NLCs on apoptosis and pyroptosis related proteins in cancer cells and tumor tissue of MFC tumor-bearing

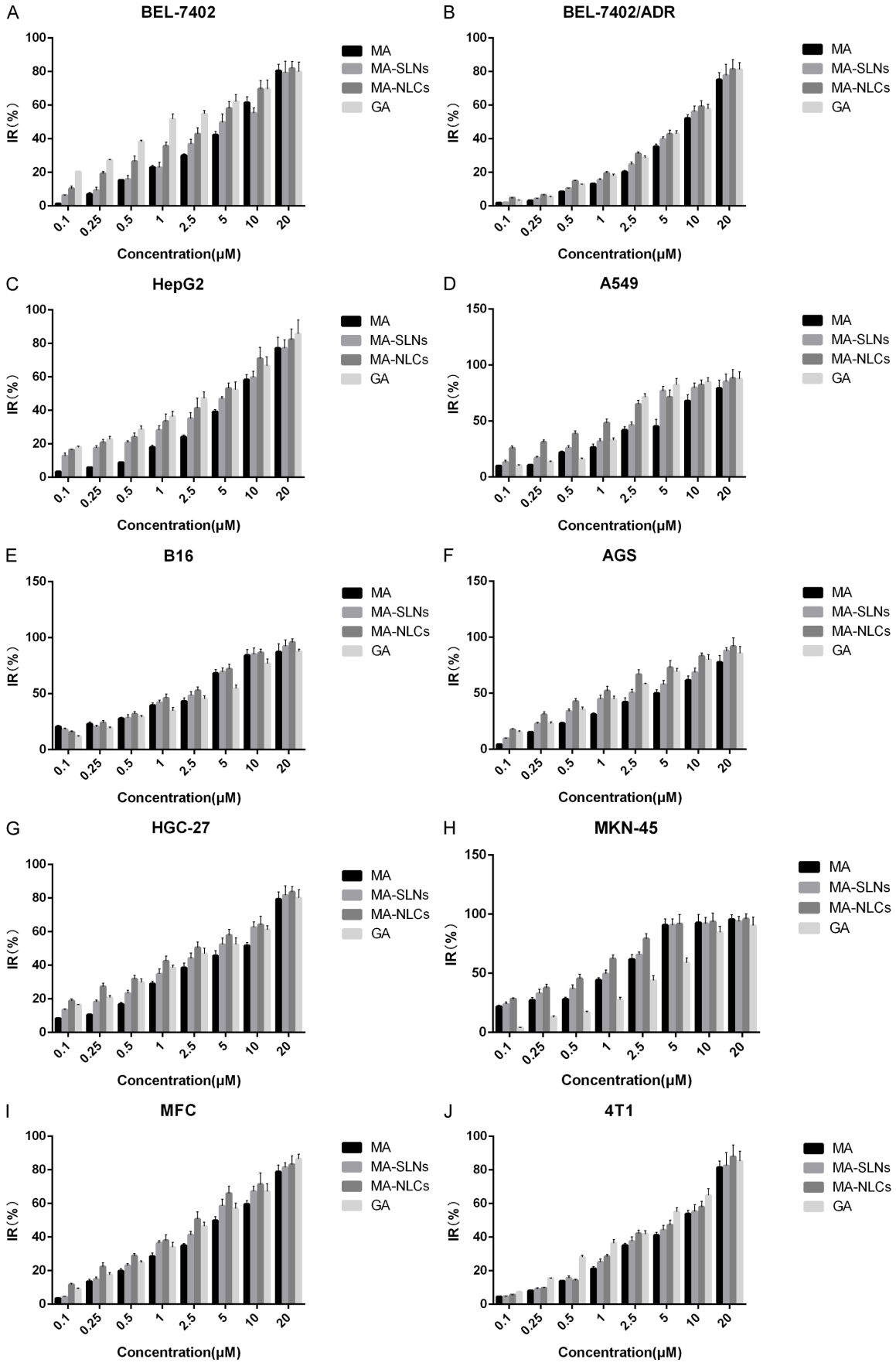
A
BEL-7402
B
BEL-7402/ADR
C
HepG2
D
A549
E
B16
F
AGS
G
HGC-27
H
MKN-45
I
MFC
J
4T1
MA
MA-SLNs
MA-NLCs
GA
IR(%)
Concentration(μM)
0.1
0.25
0.5
1
2.5
5
10
20

Figure 5. Inhibition rate of MA formulations and GA to different cancer cell lines (n=3). A. BEL-7402 cells; B. BEL-7402/ADR cells; C. HepG2 cells; D. A549 cells; E. B16 cells; F. AGS cells; G. HGC-27 cells; H. MKN-45 cells; I. MFC cells; J. 4T1 cells.

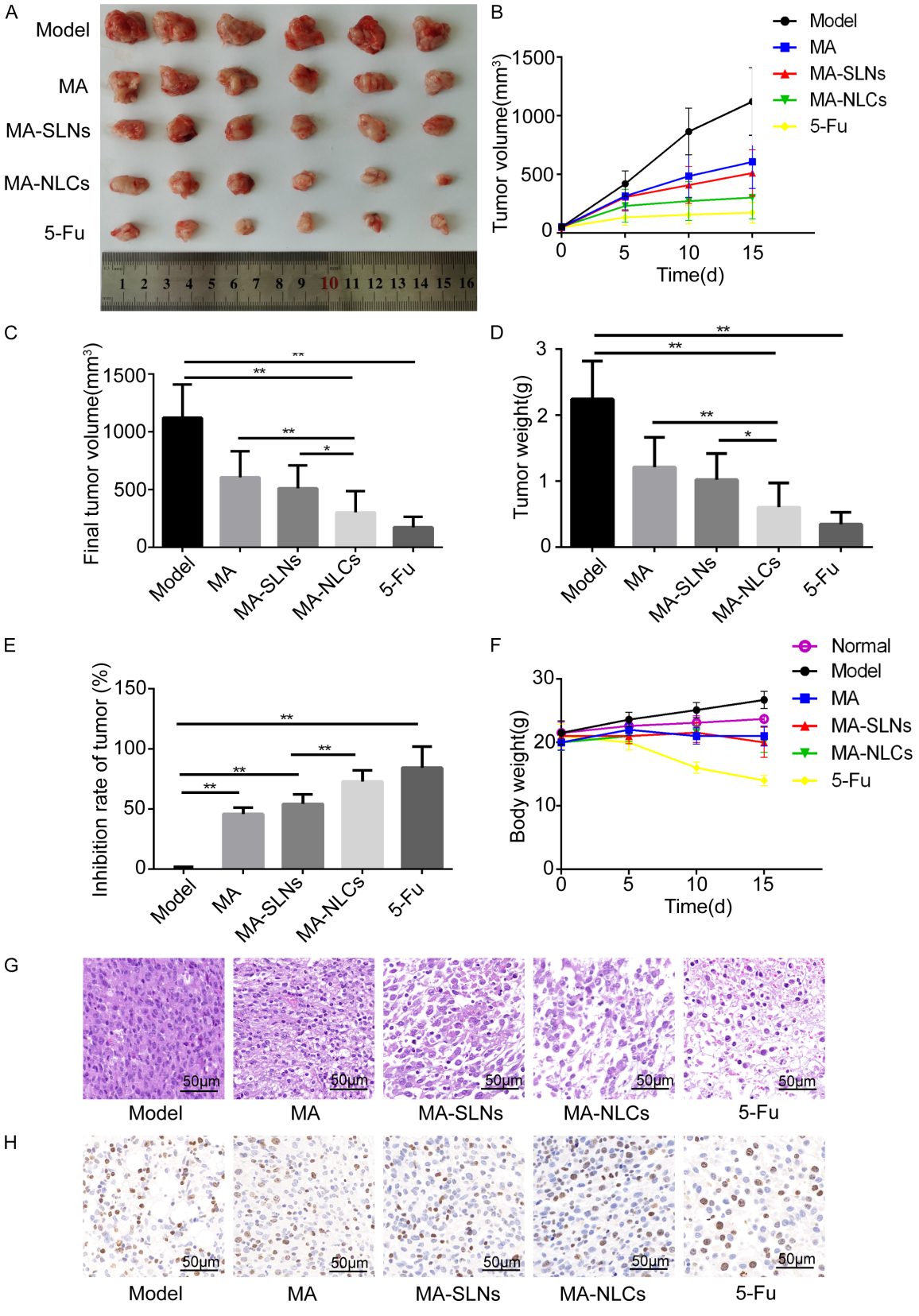

Figure 6. *In vivo* study of antitumor effect of MA formulations (n=6). A. Tumor image; B. Tumor growth curves; C. Tumor volume; D. Tumor weight; E. Inhibition rate of tumor; F. Body weight changes; G. H&E staining of tumor tissue; H. Effect of MA formulations and 5-Fu treatment on the expression of Ki67 in tumor tissue (IHC staining image, magnification: × 400). **P*<0.05, ***P*<0.01.

BALB/c mouse. The results showed that expression level of apaf-1, cleaved caspase-9 (C-cas-9), cleaved caspase-3 (C-cas-3) and GSDME-NT was remarkably increased after MA treatment (*P*<0.01 or *P*<0.05) (**Figure 7C-F**). Compared to MA group and MA-SLNs group, there was higher expression of apaf-1, C-cas-9, C-cas-3 and GSDME-NT protein in MA-NLCs group (*P*<0.01 or *P*<0.05) (**Figure 7C-F**).

Discussion

In this study, we established a simple and rapid preparative isolation method for MA. We employed an emulsification-low temperature solidification method for preparation of MA-NLCs, and an orthogonal test to optimize the preparation process. The prepared MA-NLCs showed sustained release both *in vitro* and *in vivo*. Compared with free MA solution, MA-NLCs had a higher AUC and longer half-life following i.v. administration. In addition, MA-NLCs demonstrated improved anticancer activity *in vitro* against various cancer cell lines. Furthermore, MA-NLCs displayed enhanced antitumor effect in MFC tumor-bearing BALB/c mouse model. Mechanistically, the enhanced anticancer effect of MA-NLCs *in vitro* and *in vivo* associated with its higher apoptosis and pyroptosis induction as evidenced by up-regulation of apaf-1, cleaved caspase-9, cleaved caspase-3 and GSDME-NT protein.

In our study, we employed an ultrasonic extraction method to produce a crude extract of MA, which was subsequently isolated and purified using medium-pressure semi-preparative chromatography and preparative HPLC. The purified MA were verified in line with methodologies from prior research [18]. While previous studies have extracted active compounds from Garcinia cambogia through column chromatography, these methods are often complex [2, 3]. Our approach streamlines the isolation of MA, offering a simpler and more rapid solution.

Building on previous studies [19, 20], we established an emulsion evaporation-low temperature solidification method for formulation preparation. Through one-way ANOVA and orthogonal testing, we optimized the formulation, observing that encapsulation efficiency (EE%) peaked at certain variable thresholds. However, MCT in total lipid (**Figure 2H**), proportion of drug and lipid (**Figure 2I**), amount of surfactant (**Figure 2F**), and amount of lecithin (**Figure 2K**), each increased the EE% only up to a point before diminishing. Therefore, we employed an orthogonal test to further optimize the preparation of MA-NLCs. The results indicated that the amount of MCT in total lipid significantly affected the quality of the MA-NLCs, which resulted from changes to the internal structure of NLCs caused by addition of liquid lipid. The right balance of liquid lipids can lead to a more disorganized structure, potentially enhancing drug encapsulation by creating more space within the nanoparticles [21]. The proportion of drug and lipid was another important factor that affected the quality of nanoparticles. Larger proportions of drug to lipid resulted in increased DL%, but decreased EE% [22]. Therefore, using the weighted score of the two as the evaluation index can balance the contradiction. In the next step, we characterized the MA-NLCs which were prepared using the optimized process and formulation. The prepared MA-NLCs were spherical in appearance and had particle sizes of 165.50±1.70 nm with an average PDI of 0.19±0.01. These results indicated that MA-NLCs would be unlikely to settle and could be prepared as a colloid [4]. The zeta potential of MA-NLCs was -21.85±0.67 mV, suggesting a stable formulation that resists aggregation [23]. The EE% and DL% of prepared MA-NLCs were 78.17±0.34% and 7.25±0.38%, respectively. The relatively high EE% and DL% of MA-NLCs may result from the use of solid and liquid lipids, which leads to a disordered lipid matrix with good encapsulation ability [24, 25]. In the DSC analysis, MA exhibited a sharp melting peak at 108.75°C. The melting peaks of GMS and F68 were at 62.36°C and 55.45°C, respectively. The physical mixture of individual ingredients of MA-NLCs had two additional melting peaks, which indicated an interaction between matrix and surfactants [26]. The MA-NLCs displayed a unique melting peak at 49.71°C, suggesting a homogeneous disper-

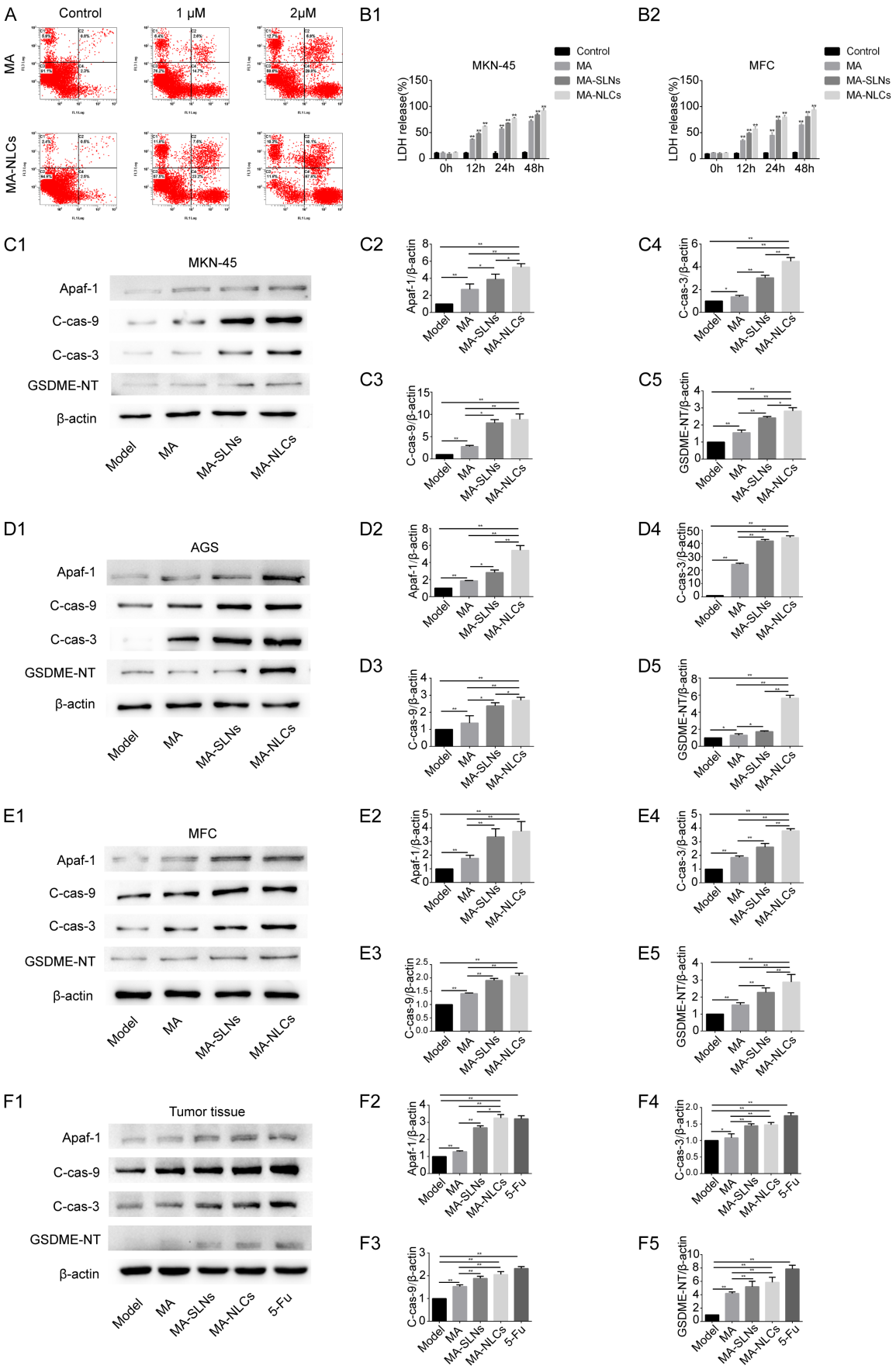
A
Control
1 μM
2μM
MA
MA-NLCs
B1
MKN-45
Control
MA
MA-SLNs
MA-NLCs
LDH release(%)
0h 12h 24h 48h
B2
MFC
C1
MKN-45
Apaf-1
C-cas-9
C-cas-3
GSDME-NT
β-actin
Model MA MA-SLNs MA-NLCs
C2
Apaf-1/β-actin
C3
C-cas-9/β-actin
C4
C-cas-3/β-actin
C5
GSDME-NT/β-actin
D1
AGS
D2
D3
D4
D5
E1
MFC
E2
E3
E4
E5
F1
Tumor tissue
Model MA MA-SLNs MA-NLCs 5-Fu
F2
F3
F4
F5

Figure 7. Study on the mechanism of antitumor effect of MA formulations (n=3). (A) Fluorescence-activated cell sorter analysis for Annexin-V and PI staining of MKN-45 cells; (B1) Effect of MA formulations on HDL release in MKN-45 cells; $^{**}P<0.01$ vs control group; (B2) Effect of MA formulations on HDL release in MFC cells; $^{**}P<0.01$ vs control group; (C1) Western blot analysis after treatment with different MA formulations for 24 h in MKN-45 cells; Expression levels of apaf-1 (C2), cleaved caspase-9 (C3), cleaved caspase-3 (C4), and GSDME-NT (C5) against β-actin in MKN-45 cells; (D1) Western blot analysis after treatment with different MA formulations for 24 h in AGS cells; Expression levels of apaf-1 (D2), cleaved caspase-9 (D3), cleaved caspase-3 (D4), and GSDME-NT (D5) against β-actin in AGS cells; (E1) Western blot analysis after treatment with different MA formulations for 24 h in MFC cells; Expression levels of apaf-1 (E2), cleaved caspase-9 (E3), cleaved caspase-3 (E4), and GSDME-NT (E5) against β-actin in MFC cells; (F1) Western blot analysis after treatment with different MA formulations and 5-Fu in tumor-bearing BALB/c mouse; Expression levels of apaf-1 (F2), cleaved caspase-9 (F3), cleaved caspase-3 (F4), and GSDME-NT (F5) against β-actin tumor tissue. $^{*}P<0.05$, $^{**}P<0.01$.

sion of MA within the NLCs and the absence of crystallization [27]. The results of stability study showed that MA-NLCs were stable at 4°C, which indicated that higher temperatures might promote gelation and drug leakage [28]. The results of *in vitro* release study showed that MA-NLCs presented a slow and sustained release property. The initial burst release of MA may have been a result of release of MA on the surface of the nanoparticles and solubilization by surfactants [29-31]. The results of *in vivo* pharmacokinetics indicated that the formulated MA-NLCs had sustained release characteristics, which correlated well with the *in vitro* release results. These findings were consistent with previous studies that incorporation of drugs in NLCs was able to overcome some of the pharmacokinetic limitations of free drugs [32-34].

Cytotoxicity assays revealed that MA-NLCs possessed superior antitumor activity *in vitro* compared to both free MA and MA-SLNs. The enhanced efficacy of MA-NLCs may be attributed to their ability to increase cell membrane permeability and promote cellular uptake, as indicated by the greater inhibition of tumor cell growth [35, 36].

Furthermore, flow cytometry results showed that both MA and MA-NLCs treatment were able to significantly induce apoptosis in tumor cell lines, with MA-NLCs proving more potent. In previous studies, other components with anticancer efficacy from Garcinia hanburyi were also found to have activity of inducing cancer cells apoptosis [37, 38]. The increased apoptosis observed with MA post-encapsulation in NLCs also corroborates earlier research [39, 40].

The results of antitumor study showed that MA could significantly inhibit tumor growth *in vivo*, and the encapsulation of NLCs could enhance its antitumor effect. This could be due to the enhanced permeability and retention (EPR) effect of the nanocarriers, which enables nanoparticles, particularly those sized between 100-200 nm, to be preferentially retained in tumor tissues, thereby increasing local drug concentration and effecting passive targeting [41]. Notably, there was no significant weight loss in the MA dose groups, while body weight in 5-Fu group was significantly reduced, reflecting the higher safety of MA compared with traditional chemotherapeutic drugs. H&E staining results showed that the tumor cells in animal tumor tissues of the model group had intact nuclei and were densely arranged, while apoptotic and necrotic cells could be seen in the tumor tissues of MA formulations group and the 5-Fu group. The results of IHC suggested that Ki67 expression in the tumor tissues of MA formulations and the 5-Fu group was significantly lower than that in the model group. These results suggest that the inhibitory effect of MA on cancer *in vivo* may result from its inhibition of cell proliferation and apoptosis induction.

Moreover, our investigation delved into the impact of MA on apoptosis and pyroptosis-associated proteins within tumor cells and tissues. Our experimental findings revealed a significant upregulation of cleaved caspase-9, cleaved caspase-3, and GSDME-NT by MA formulations. The results suggested a potential antitumor effect of MA by inducing of caspase-3-mediated apoptosis and pyroptosis within tumor cells. Specifically, MA acted on the mitochondrial membrane to affect Bcl-2 family protein thereby increasing the release of cytochrome C upon receipt of apoptotic signals. Once released from mitochondria, cytochrome C interacted Apaf-1, formed an active complex

with caspase-9 to activate caspase-3, which initiates apoptosis [42]. Additionally, cleaved caspase-3 can cleave GSDME to produce GSDME-NT, which forms pores in cell membranes, leading to pyroptosis [43]. These findings align with previous research on the antitumor properties of active compounds found in Garcinia plants. GA demonstrated the ability to induce apoptosis in esophageal squamous cell carcinoma cells in a dose-dependent manner, which was achieved by reducing Bcl-2 levels and increasing the levels of Bax, cleaved-PARP1 and cleaved caspase 3/9 [44]. In a study involving gastric signet ring cell carcinoma, GA revealed an upregulation of cleaved caspase 3, Bax, and cleaved PARP, along with a downregulation of Bcl-2 [45]. GA-loaded NLCs have also been reported to inhibit tumor and metastasis growth, potentially due to alterations in MMP-9, BCL-2, and E-cadherin levels [46], and GA has been found to influence the expression of Bax, caspase 3, and caspase 9 in human osteosarcoma [47].

In summary, MA-NLCs, as a novel drug delivery system, substantially increase MA's solubility, circulation time, tissue selectivity, and anticancer efficacy, while reducing toxicity. NLCs also safeguard the drug from biological degradation, thereby enhancing its stability [48]. While previous studies indicate that NLCs contribute to improved oral absorption and enhanced bioavailability of drugs [49], MA-NLCs still face certain limitations, such as potential nanomaterial toxicity and the absence of comprehensive clinical safety data. NLCs belong to thermodynamically unstable systems, posing significant challenges in the storage and transportation of MA-NLCs [50]. Moreover, achieving precise drug targeting to cater to various anatomical and pathological tumor characteristics remains an ongoing challenge.

Ultimately, MA-NLCs have shown a remarkable increase in efficacy against cancer cells *in vitro*, as well as significant suppressive effects on tumor growth *in vivo*. Consequently, MA-NLCs may pave the way for groundbreaking advancements in anticancer drug research and hold promise for future clinical applications in cancer therapy.

Acknowledgements

This work was supported by the National Natural Science Foundation of China (81773-988), National Key New Drugs Creation Project (52-401013), Scientific Research Project of Anhui Higher Education Institutions (2022-AH050450), Talent Support Program of Anhui University of Chinese Medicine (2022rcyb002 and 2022rcyb007) and Natural Science Research Projects Program of Anhui University of Chinese Medicine (2021zrzd05 and 2021zrzd16).

Disclosure of conflict of interest

None.

Address correspondence to: Guangliang Chen, College of Integrative Medicine, Anhui University of Chinese Medicine, Hefei, Anhui, China. E-mail: chen_guangl@126.com; Weidong Chen, College of Pharmacy, Anhui University of Chinese Medicine, Hefei, Anhui, China. E-mail: wdchen@ahtcm.edu.cn

References

[1] Jia B, Li S, Hu X, Zhu G and Chen W. Recent research on bioactive xanthones from natural medicine: Garcinia hanburyi. AAPS PharmSciTech 2015; 16: 742-758.

[2] Ren Y, Lantvit DD, Carcache de Blanco EJ, Kardono LB, Riswan S, Chai H, Cottrell CE, Farnsworth NR, Swanson SM, Ding Y, Li XC, Marais JP, Ferreira D and Kinghorn AD. Proteasome-inhibitory and cytotoxic constituents of Garcinia lateriflora: absolute configuration of caged xanthones. Tetrahedron 2010; 66: 5311-5320.

[3] Reutrakul V, Anantachoke N, Pohmakotr M, Jaipetch T, Sophasan S, Yoosook C, Kasisit J, Napaswat C, Santisuk T and Tuchinda P. Cytotoxic and anti-HIV-1 caged xanthones from the resin and fruits of Garcinia hanburyi. Planta Med 2007; 73: 33-40.

[4] Yang J, He S, Li S, Zhang R, Peng A and Chen L. In vitro and in vivo antiangiogenic activity of caged polyprenylated xanthones isolated from Garcinia hanburyi Hook. f. Molecules 2013; 18: 15305-15313.

[5] Li Y, Zhang Q and Jiang D. Validation of an HPLC-MS-MS assay for determination of morellic acid in rat plasma: application to pharmacokinetic studies. J Chromatogr Sci 2015; 53: 1695-1700.

[6] Yang G, Wu F, Chen M, Jin J, Wang R and Yuan Y. Formulation design, characterization, and in vitro and in vivo evaluation of nanostructured lipid carriers containing a bile salt for oral delivery of gypenosides. Int J Nanomedicine 2019; 14: 2267-2280.

[7] Negi LM, Jaggi M and Talegaonkar S. A logical approach to optimize the nanostructured lipid

carrier system of irinotecan: efficient hybrid design methodology. Nanotechnology 2013; 24: 015104.
[8] Huang X, Chen YJ, Peng DY, Li QL, Wang XS, Wang DL and Chen WD. Solid lipid nanoparticles as delivery systems for Gambogenic acid. Colloids Surf B Biointerfaces 2013; 102: 391-397.
[9] Hu H, Liu D, Zhao X, Qiao M and Chen D. Preparation, characterization, cellular uptake and evaluation in vivo of solid lipid nanoparticles loaded with cucurbitacin B. Drug Dev Ind Pharm 2013; 39: 770-779.
[10] Song J, Fan X and Shen Q. Daidzein-loaded nanostructured lipid carriers-PLGA nanofibers for transdermal delivery. Int J Pharm 2016; 501: 245-252.
[11] Kraisit P and Sarisuta N. Development of triamcinolone acetonide-loaded nanostructured lipid carriers (NLCs) for buccal drug delivery using the box-behnken design. Molecules 2018; 23: 982.
[12] Zhao S, Minh LV, Li N, Garamus VM, Handge UA, Liu J, Zhang R, Willumeit-Römer R and Zou A. Doxorubicin hydrochloride-oleic acid conjugate loaded nanostructured lipid carriers for tumor specific drug release. Colloids Surf B Biointerfaces 2016; 145: 95-103.
[13] Hassanzadeh P, Atyabi F, Dinarvand R, Dehpour AR, Azhdarzadeh M and Dinarvand M. Application of nanostructured lipid carriers: the prolonged protective effects for sesamol in in vitro and in vivo models of ischemic stroke via activation of PI3K signalling pathway. Daru 2017; 25: 25.
[14] Shi F, Zhao Y, Firempong CK and Xu X. Preparation, characterization and pharmacokinetic studies of linalool-loaded nanostructured lipid carriers. Pharm Biol 2016; 54: 2320-2328.
[15] Managuli RS, Wang JT, Faruqu FN, Kushwah V, Raut SY, Shreya AB, Al-Jamal KT, Jain S and Mutalik S. Asenapine maleate-loaded nanostructured lipid carriers: optimization and in vitro, ex vivo and in vivo evaluations. Nanomedicine (Lond) 2019; 14: 889-910.
[16] Kang Q, Liu J, Zhao Y, Liu X, Liu XY, Wang YJ, Mo NL and Wu Q. Transdermal delivery system of nanostructured lipid carriers loaded with celastrol and indomethacin: optimization, characterization and efficacy evaluation for rheumatoid arthritis. Artif Cells Nanomed Biotechnol 2018; 46: S585-S597.
[17] Sabzichi M, Mohammadian J, Mohammadi M, Jahanfar F, Movassagh Pour AA, Hamishehkar H and Ostad-Rahimi A. Vitamin D-loaded nanostructured lipid carrier (NLC): a new strategy for enhancing efficacy of doxorubicin in breast cancer treatment. Nutr Cancer 2017; 69: 840-848.
[18] Zhou Y, Liu X, Yang J, Han QB, Song JZ, Li SL, Qiao CF, Ding LS and Xu HX. Analysis of caged xanthones from the resin of Garcinia hanburyi using ultra-performance liquid chromatography/electrospray ionization quadrupole time-of-flight tandem mass spectrometry. Anal Chim Acta 2008; 629: 104-118.
[19] Chen-yu G, Chun-fen Y, Qi-lu L, Qi T, Yan-wei X, Wei-na L and Guang-xi Z. Development of a quercetin-loaded nanostructured lipid carrier formulation for topical delivery. Int J Pharm 2012; 430: 292-298.
[20] Wang Q, Cheng H, Zhou K, Wang L, Dong S, Wang D and Chen W. Nanostructured lipid carriers as a delivery system of biochanin A. Drug Deliv 2013; 20: 331-337.
[21] Niculae G, Badea N, Meghea A, Oprea O and Lacatusu I. Coencapsulation of butyl-methoxydibenzoylmethane and octocrylene into lipid nanocarriers: UV performance, photostability and in vitro release. Photochem Photobiol 2013; 89: 1085-1094.
[22] Varshosaz J, Sadeghi H, Andalib S and Hassanzadeh F. Optimization of LDL targeted nanostructured lipid carriers of 5-FU by a full factorial design. Adv Biomed Res 2012; 1: 45.
[23] Chanburee S and Tiyaboonchai W. Mucoadhesive nanostructured lipid carriers (NLCs) as potential carriers for improving oral delivery of curcumin. Drug Dev Ind Pharm 2017; 43: 432-440.
[24] Shinde UA, Parmar SJ and Easwaran S. Metronidazole-loaded nanostructured lipid carriers to improve skin deposition and retention in the treatment of rosacea. Drug Dev Ind Pharm 2019; 45: 1039-1051.
[25] Kasongo KW, Pardeike J, Muller RH and Walker RB. Selection and characterization of suitable lipid excipients for use in the manufacture of didanosine-loaded solid lipid nanoparticles and nanostructured lipid carriers. J Pharm Sci 2011; 100: 5185-5196.
[26] Seyfoddin A and Al-Kassas R. Development of solid lipid nanoparticles and nanostructured lipid carriers for improving ocular delivery of acyclovir. Drug Dev Ind Pharm 2013; 39: 508-519.
[27] Nair R, Priya KV, Kumar KSA, Badivaddin TM and Sevukarajan M. Formulation and evaluation of solid lipid nanoparticles of water soluble drug: isoniazid. J Pharm Sci Res 2011; 3: 1256-1264.
[28] Kanwar R, Gradzielski M, Prevost S, Appavou MS and Mehta SK. Experimental validation of biocompatible nanostructured lipid carriers of sophorolipid: optimization, characterization and in-vitro evaluation. Colloids Surf B Biointerfaces 2019; 181: 845-855.
[29] Rohit B and Pal KI. A method to prepare solid lipid nanoparticles with improved entrapment

efficiency of hydrophilic drugs. Current Nanoscience 2013; 9: 211-220.
[30] Singh S, Dobhal AK, Jain A, Pandit JK and Chakraborty S. Formulation and evaluation of solid lipid nanoparticles of a water soluble drug: zidovudine. Chem Pharm Bull (Tokyo) 2010; 58: 650-655.
[31] Selvaraj K and Yoo BK. Curcumin-loaded nanostructured lipid carrier modified with partially hydrolyzed ginsenoside. AAPS PharmSciTech 2019; 20: 252.
[32] Olbrich C, Kayser O and Muller RH. Lipase degradation of dynasan 114 and 116 solid lipid nanoparticles (SLN)--effect of surfactants, storage time and crystallinity. Int J Pharm 2002; 237: 119-128.
[33] Olbrich C and Muller RH. Enzymatic degradation of SLN-effect of surfactant and surfactant mixtures. Int J Pharm 1999; 180: 31-39.
[34] Muchow M, Maincent P, Muller RH and Keck CM. Production and characterization of testosterone undecanoate-loaded NLC for oral bioavailability enhancement. Drug Dev Ind Pharm 2011; 37: 8-14.
[35] Guo S, Zhang Y, Wu Z, Zhang L, He D, Li X and Wang Z. Synergistic combination therapy of lung cancer: cetuximab functionalized nanostructured lipid carriers for the co-delivery of paclitaxel and 5-Demethylnobiletin. Biomed Pharmacother 2019; 118: 109225.
[36] Lu Z, Su J, Li Z, Zhan Y and Ye D. Hyaluronic acid-coated, prodrug-based nanostructured lipid carriers for enhanced pancreatic cancer therapy. Drug Dev Ind Pharm 2017; 43: 160-170.
[37] Pan H, Lu LY, Wang XQ, Li BX, Kelly K and Lin HS. Gambogic acid induces cell apoptosis and inhibits MAPK pathway in $PTEN^{-/-}/p53^{-/-}$ prostate cancer cells in vitro and ex vivo. Chin J Integr Med 2018; 24: 109-116.
[38] Su J, Xu T, Jiang G, Hou M, Liang M, Cheng H and Li Q. Gambogenic acid triggers apoptosis in human nasopharyngeal carcinoma CNE-2Z cells by activating volume-sensitive outwardly rectifying chloride channel. Fitoterapia 2019; 133: 150-158.
[39] Xu W, Wang H, Dong L, Zhang P, Mu Y, Cui X, Zhou J, Huo M and Yin T. Hyaluronic acid-decorated redox-sensitive chitosan micelles for tumor-specific intracellular delivery of gambogic acid. Int J Nanomedicine 2019; 14: 4649-4666.
[40] Tang X, Sun J, Ge T, Zhang K, Gui Q, Zhang S and Chen W. PEGylated liposomes as delivery systems for Gambogenic acid: characterization and in vitro/in vivo evaluation. Colloids Surf B Biointerfaces 2018; 172: 26-36.
[41] Shi Y, van der Meel R, Chen X and Lammers T. The EPR effect and beyond: strategies to improve tumor targeting and cancer nanomedicine treatment efficacy. Theranostics 2020; 10: 7921-7924.
[42] Qin XY, Wang YN, Liu HF, Luo ZH, Zhang PL, Li-Fang H and Liu MR. Anti-cancer activities of metal-based complexes by regulating the VEGF/VEGFR2 signaling pathway and apoptosis-related factors Bcl-2, Bax, and caspase-9 to inhibit angiogenesis and induce apoptosis. Metallomics 2020; 12: 92-103.
[43] Hu L, Chen M, Chen X, Zhao C, Fang Z, Wang H and Dai H. Chemotherapy-induced pyroptosis is mediated by BAK/BAX-caspase-3-GSDME pathway and inhibited by 2-bromopalmitate. Cell Death Dis 2020; 11: 281.
[44] Yu J, Wang W, Yao W, Yang Z, Gao P, Liu M, Wang H, Chen S, Wang D, Wang W and Sun G. Gambogic acid affects ESCC progression through regulation of PI3K/AKT/mTOR signal pathway. J Cancer 2020; 11: 5568-5577.
[45] Joha Z, Öztürk A, Yulak F, Karataş Ö and Ataseven H. Mechanism of anticancer effect of gambogic acid on gastric signet ring cell carcinoma. Med Oncol 2023; 40: 269.
[46] Dang W, Xing B, Jia X, Zhang Y, Jia B, Yu C, He J, Li Z, Li H and Liu Z. Subcellular organelle-targeted nanostructured lipid carriers for the treatment of metastatic breast cancer. Int J Nanomedicine 2023; 18: 3047-3068.
[47] Liu Z, Wang X, Li J, Yang X, Huang J, Ji C, Li X, Li L, Zhou J and Hu Y. Gambogenic acid induces cell death in human osteosarcoma through altering iron metabolism, disturbing the redox balance, and activating the P53 signaling pathway. Chem Biol Interact 2023; 382: 110602.
[48] Alcantara KP, Zulfakar MH and Castillo AL. Development, characterization and pharmacokinetics of mupirocin-loaded nanostructured lipid carriers (NLCs) for intravascular administration. Int J Pharm 2019; 571: 118705.
[49] Hassan DH, Shohdy JN, El-Setouhy DA, El-Nabarawi M and Naguib MJ. Compritol-based nanostrucutured lipid carriers (NLCs) for augmentation of zolmitriptan bioavailability via the transdermal route: In vitro optimization, ex vivo permeation, in vivo pharmacokinetic study. Pharmaceutics 2022; 14: 1484.
[50] Neves AR, Lúcio M, Martins S, Lima JL and Reis S. Novel resveratrol nanodelivery systems based on lipid nanoparticles to enhance its oral bioavailability. Int J Nanomedicine 2013; 8: 177-87.